JACS
JOURNAL OF THE AMERICAN CHEMICAL SOCIETY
Communication
pubs.acs.org/JACS

Large-Area Synthesis of High-Quality Uniform Few-Layer $MoTe_2$

Lin Zhou,[†] Kai Xu,[†,‡] Ahmad Zubair,[†] Albert D. Liao,[†] Wenjing Fang,[†] Fangping Ouyang,[†,§] Yi-Hsien Lee,[∥] Keiji Ueno,[⊥] Riichiro Saito,[#] Tomás Palacios,[†] Jing Kong,[*,†] and Mildred S. Dresselhaus[*,†,∇]

[†]Department of Electrical Engineering and Computer Science, Massachusetts Institute of Technology, Cambridge, Massachusetts 02139, United States

[‡]State Key Laboratory of Heavy Oil Processing, China University of Petroleum, Beijing 102249, China

[§]School of Physics and Electronics, State Key Laboratory of Powder Metallurgy, Central South University, Changsha 410083, China

[∥]Material Sciences and Engineering, National Tsing-Hua University, Hsinchu 30013, Taiwan

[⊥]Department of Chemistry, Graduate School of Science and Engineering, Saitama University, Saitama 338-8570, Japan

[#]Department of Physics, Tohoku University, Sendai 980-8578, Japan

[∇]Department of Physics, Massachusetts Institute of Technology, Cambridge, Massachusetts 02139, United States

Supporting Information

ABSTRACT: The controlled synthesis of large-area, atomically thin molybdenum ditelluride ($MoTe_2$) crystals is crucial for its various applications based on the attractive properties of this emerging material. In this work, we developed a chemical vapor deposition synthesis to produce large-area, uniform, and highly crystalline few-layer 2H and 1T′ $MoTe_2$ films. It was found that these two different phases of $MoTe_2$ can be grown depending on the choice of Mo precursor. Because of the highly crystalline structure, the as-grown few-layer 2H $MoTe_2$ films display electronic properties that are comparable to those of mechanically exfoliated $MoTe_2$ flakes. Our growth method paves the way for the large-scale application of $MoTe_2$ in high-performance nanoelectronics and optoelectronics.

Two-dimensional transition metal dichalcogenides (TMDs) have been attracting increasing interest because of their unique structures and remarkable properties, which make them promising materials for a wide range of applications related to, e.g., electronics,[1−3] optoeletronics,[4−6] valleytronics,[7] spintronics,[8] and catalysis.[9,10] As a member of the TMD family, $MoTe_2$ possesses interesting features. Bulk $MoTe_2$ has an indirect band gap of ~1.0 eV, and single-layer $MoTe_2$ is a direct-gap semiconductor with an optical band gap of 1.1 eV.[11] Because of the smaller band gap compared with other group 6 TMDs, single- and few-layer $MoTe_2$ holds promise for use in easily controllable ambipolar field-effect transistors (FETs) and extends the operating range of TMD optoelectronic devices from the visible to the near-infrared range.[11−13] In particular, the band gap, which is quite close to that of Si (~1.1 eV), the strong absorption throughout solar spectrum,[14] and the strong spin−orbit coupling suggest that $MoTe_2$ is a highly attractive material for use in electronic devices, photovoltaic devices, and spintronic and valley-optoelectronic devices.[11,12]

A crucial step toward the practical application of $MoTe_2$ in electronics and optoelectronics is the controlled production of high-quality, large-area, atomically thin $MoTe_2$ films. To date, single- and few-layer $MoTe_2$ have only been achieved using "top-down" exfoliation methods.[12,15] However, exfoliation produces only small $MoTe_2$ flakes with arbitrary shape that are randomly distributed on a surface, thus preventing production for large-scale applications. Liquid exfoliation is a promising method for mass production of atomically thin $MoTe_2$,[15] but the low quality of $MoTe_2$ obtained using this technique cannot satisfy the requirements for electronic and optoelectronic applications. Therefore, a technology for the mass production of high-quality, large-area, atomically thin $MoTe_2$ films is highly desirable.

Compared with other group 6 TMD materials, stoichiometric $MoTe_2$ films are more difficult to achieve. The electronegativity difference between Te and Mo is much smaller (0.3 eV) among these materials. Therefore, the bonding energy of Mo−Te bonds is quite small, which translates to a weaker tendency for the material to form and difficulty in obtaining stoichiometric $MoTe_2$. Moreover, at high temperatures, instead of evaporating as a compound, $MoTe_2$ decomposes and loses Te as a vapor. These properties make it challenging to directly obtain atomically thin $MoTe_2$ films by physical vapor deposition, and there is very often a Te deficiency in as-prepared $MoTe_2$.

In regard to the synthesis of $MoTe_2$, another unique feature distinguishing $MoTe_2$ from other TMDs is the small energy difference (<0.1 eV per $MoTe_2$ unit) between the two crystal phases of $MoTe_2$, i.e., the semiconducting 2H and metallic 1T′ phases.[16] As a result, $MoTe_2$ can be reversibly switched from the 2H phase to the 1T′ phase by changing the temperature,[17] which on one hand makes it a promising two-dimensional material for phase-change memory applications but on the other hand poses challenges for the controllable synthesis of a pure $MoTe_2$ crystal phase. In this work, we investigated the synthesis of $MoTe_2$ via chemical vapor deposition (CVD) and found that pure 2H and pure 1T′ $MoTe_2$ films can be selectively synthesized by selecting different Mo precursors. The resulting 2H $MoTe_2$ films can be as thin as a few atomic layers, with high crystalline quality and

Received: July 16, 2015
Published: August 25, 2015

 © 2015 American Chemical Society
DOI: 10.1021/jacs.5b07452
J. Am. Chem. Soc. 2015, 137, 11892−11895

excellent electrical characteristics comparable to those of exfoliated samples.

The strategy for the synthesis of $MoTe_2$ films is schematically illustrated in Figure 1a. Briefly, a 1 nm Mo film was deposited onto a SiO_2/Si substrate by electron beam evaporation. Then the Mo film was fully oxidized in air to give MoO_3. The resulting MoO_3 film was placed in a ceramic crucible containing Te powder. A mixture of argon and hydrogen (3 sccm Ar, 4 sccm H_2) was used as the carrier gas and formed a reducing atmosphere during the CVD growth. Hydrogen was essential for the $MoTe_2$ growth, similar to the growth of Se-based TMD materials.[18] Molecular sieves were added to the crucible before growth and were found to absorb byproducts during growth and to help release Te vapor in a controllable way. The growth temperature was controlled at 700 °C (Figure 1b). The MoO_3 film was tellurized into a $MoTe_2$ film after annealing in Te vapor at this temperature. Figure 1c shows a typical optical image of an as-synthesized $MoTe_2$ film. The film is uniform and continuous across the whole area (~1 cm), as can be seen from the homogeneous color contrast in the image.

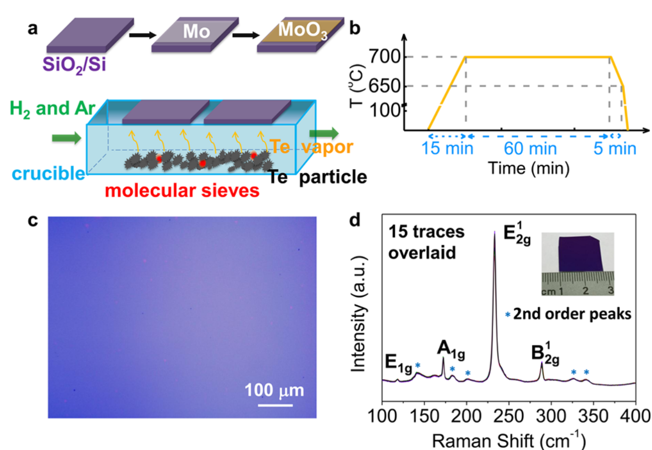

Figure 1. Synthesis of 2H $MoTe_2$. (a) Schematic illustration of the $MoTe_2$ CVD process. (b) Temperature-controlled sequence typically used for growth of $MoTe_2$. (c) Typical optical image of an as-synthesized $MoTe_2$ film on a 300 nm SiO_2/Si substrate. (d) Raman spectra of a $MoTe_2$ film taken at 15 different locations on the sample. Inset: Photograph of a $MoTe_2$ film on a 1.6 cm × 1.8 cm SiO_2/Si substrate.

The crystal quality and uniformity of few-layer $MoTe_2$ films were further characterized by Raman spectroscopy using a 532 nm excitation laser. To investigate the spatial variations of the CVD-grown film on a scale of a few centimeters, Raman spectra were collected at 15 randomly chosen positions on the sample (Figure 1d). The $MoTe_2$ film shows several Raman peaks between 100 and 400 cm^{-1}: the in-plane E_{1g} mode at ~119 cm^{-1}, the out-of-plane A_{1g} mode at ~171 cm^{-1}, the prominent peak of the in-plane E^1_{2g} mode at ~234 cm^{-1}, and the out-of-plane B^1_{2g} mode at ~289 cm^{-1}. Besides these first-order Raman peaks, several second-order resonant peaks with relatively low intensities at ~140, 183, 204, 327, and 344 cm^{-1} are also observed. These Raman features coincide with those observed in few-layer 2H $MoTe_2$ and thus unequivocally identify the as-grown film as 2H $MoTe_2$.[19,20] The presence of the B^1_{2g} peak at ~289 cm^{-1} indicates that the synthesized film is atomically thin, since the B^1_{2g} mode is Raman-inactive in single-layer and bulk 2H $MoTe_2$.[19] Additionally, the nearly identical positions and intensities of the peaks in these Raman spectra taken at all of these locations strongly suggest that the CVD-grown large-area atomically thin $MoTe_2$ film (1.6 × 1.8 cm^2) is highly homogeneous.

Micro-Raman mapping was performed to evaluate the uniformity of the $MoTe_2$ film. The intensity map of the E^1_{2g} peak (Figure 2b), the A_{1g} peak (Figure 2c), and the B^1_{2g} peak (Figure 2d) of the $MoTe_2$ film (Figure 2a) all show uniformly distributed color, indicating the high homogeneity of the $MoTe_2$ film within the spatial resolution of the Raman instrument (~1 μm). The ratio of the intensities of the B^1_{2g} and E^1_{2g} peaks is sensitive to the thickness of the $MoTe_2$ film and decreases as the number of $MoTe_2$ layers increases.[19] The homogeneity in color presented in the intensity ratio map (Figure 2e) further confirms that the thickness of the $MoTe_2$ film is uniform over the whole mapping area. Atomic force microscopy (AFM) images of the grown film on the edge (Figure 2f) reveal that the $MoTe_2$ is a uniform thin film with a height of ~3.1 nm. The $MoTe_2$ surface has a roughness of 0.3 nm, which is similar to that of the SiO_2 substrate, further indicating that a high-quality material was grown. Since the interlayer spacing in $MoTe_2$ is about 0.7 nm,[12] our grown film (Figure 2f) should be a four-layer film of $MoTe_2$.

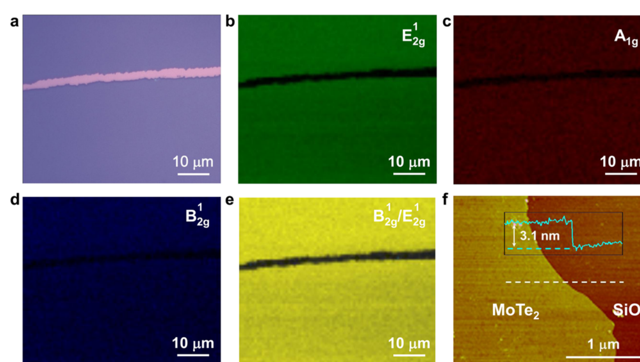

Figure 2. Uniformity of the $MoTe_2$ characterized via Raman mapping and AFM. (a) Optical microscope image of a $MoTe_2$ region, with a scratch line showing the bare SiO_2 substrate (pink line). (b−d) Raman intensity mapping of (b) the E^1_{2g} peak, (c) the A_{1g} peak, and (d) the B^1_{2g} peak and (e) the B^1_{2g}/E^1_{2g} intensity ratio map taken from the $MoTe_2$ region shown in (a). (f) AFM image of the CVD-grown $MoTe_2$. The height profile (inset) indicates that the film has a thickness of 3.1 nm.

X-ray photoelectron spectroscopy (XPS) was utilized to examine the elemental composition and bonding types in the CVD-grown film. The XPS survey spectra reveal the presence of Mo and Te elements that originate from the $MoTe_2$ film (Figure S1). The prominent Mo 3d peaks at 228.3 eV ($3d_{5/2}$) and 231.5 eV ($3d_{3/2}$) are assigned to Mo−Te bonds (Figure 3a).[21] The Te $3d_{5/2}$ and $3d_{3/2}$ peaks, located at 573 and 583.4 eV, respectively, are also attributed to Mo−Te bonds (Figure 3b).[21] These features are consistent with the XPS spectra obtained from a bulk $MoTe_2$ crystal. Additionally, the Mo:Te atomic ratio is 1:2.02, indicating that the CVD-grown $MoTe_2$ film is stoichiometric.

The crystallographic structure and the chemical composition of the $MoTe_2$ film were further characterized by transmission electron microscopy (TEM), selected-area electron diffraction (SAED), and energy-dispersive X-ray spectrometry (EDX). Figure 3c shows a typical TEM image of our $MoTe_2$ film. The continuity of the film suggests that our CVD-grown $MoTe_2$ film is of high quality. Figure 3e displays the SAED pattern which shows the hexagonal symmetry of the CVD-grown $MoTe_2$. SAED patterns taken at several locations on this sample revealed

DOI: 10.1021/jacs.5b07452
J. Am. Chem. Soc. 2015, 137, 11892−11895

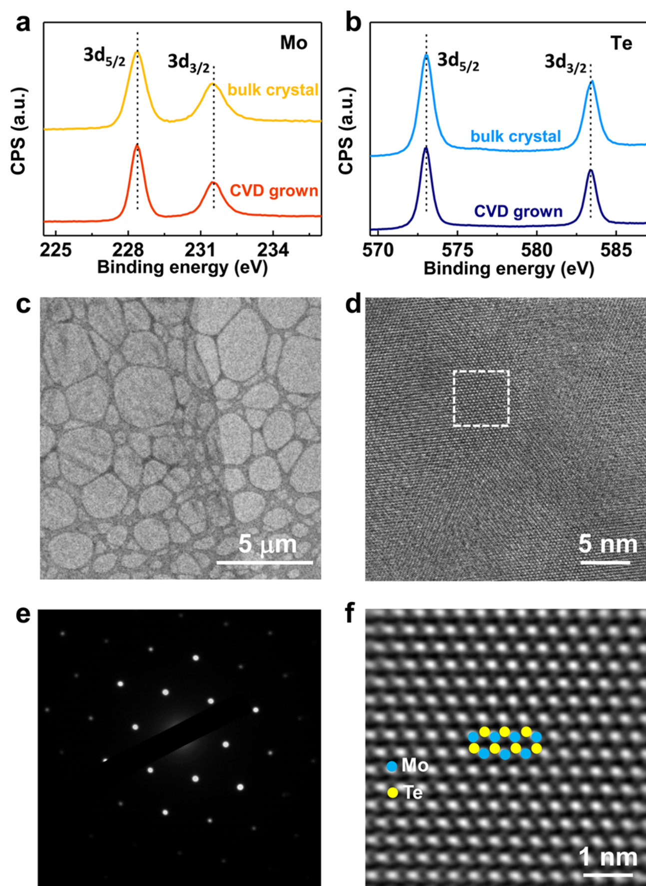

Figure 3. XPS and TEM characterizations of a 2H $MoTe_2$ film. (a) XPS spectra of Mo 3d core levels for the CVD-grown $MoTe_2$ film (red) and the bulk $MoTe_2$ crystal (yellow). (b) High-resolution Te 3d XPS spectra of the same region on the $MoTe_2$ film (blue) and the bulk $MoTe_2$ crystal (cyan). (c) Low-resolution TEM image of the CVD-grown $MoTe_2$ film supported on a TEM grid. (d) High-resolution TEM image of the same $MoTe_2$ film. (e) Corresponding SAED pattern. (f) FFT-filtered image of the area marked in (d). The inset shows the overlay of an atomic structure model of $MoTe_2$.

hexagonal patterns with the same orientations (Figure S2), indicating that the lateral crystal domain size of this $MoTe_2$ specimen can reach up to 30 μm, comparable to that of exfoliated $MoTe_2$.[13] High-resolution TEM shows a hexagonal atomic lattice of alternating bright and dark spots with a lattice spacing of 0.35 nm, which is consistent with the structure of 2H $MoTe_2$ (Figure 3f). The EDX spectrum reveals that the as-grown film contains Mo and Te (Figure S3).

Transport measurements were used to characterize the electrical properties of our few-layer $MoTe_2$ film. The large-area, uniform, and atomically thin $MoTe_2$ film greatly facilitated the fabrication of electrical devices. FET devices with various channel lengths from 300 nm to 6.5 μm were fabricated on a Si/SiO_2 substrate using electron-beam lithography (EBL) followed by metal deposition (1 nm Ti/60 nm Au). After EBL, the $MoTe_2$ devices were tailored into bars with a width of 20 μm using a reactive ion etching process (Figure 4a). The nonlinear $I_{ds}-V_{ds}$ characteristics suggest that Schottky contacts are formed between the Ti/Au metal pads and $MoTe_2$ (Figure 4b). The $MoTe_2$ device exhibits p-type conduction with an ON/OFF current ratio of $\sim 10^3$ and an estimated carrier concentration of $>4.8 \times 10^{12}$ cm^{-2} (Figure 4d). Unlike other group 6 TMDs (MoS_2, $MoSe_2$, WS_2), which usually behave as n-type semi-

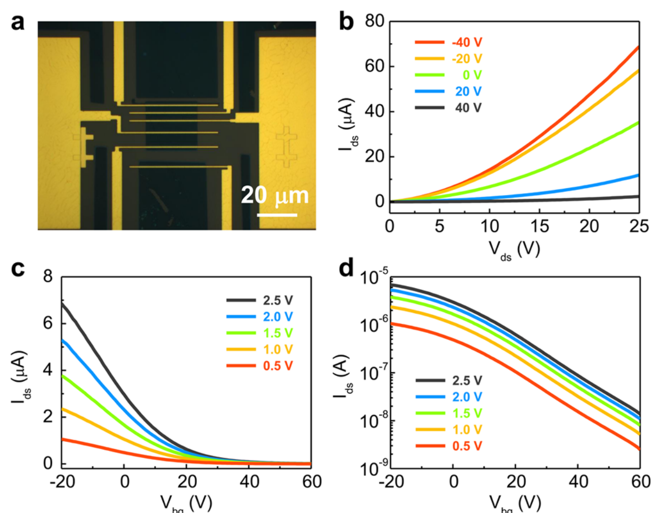

Figure 4. Electrical properties of devices made from a 2H $MoTe_2$ film. (a) Typical optical image of a $MoTe_2$ device on 90 nm SiO_2/Si. The darker region is $MoTe_2$. In the following, the channel length and width of this FET are ~6.5 and 20.0 μm, respectively. (b) Output characteristics (I_{ds} vs V_{ds}) of our $MoTe_2$ FET device at various values of the gate voltage (V_{bg}). (c, d) Transfer characteristics (I_{ds} vs V_{bg}) curves for the same devices at various value of V_{ds} on (c) linear and (d) logarithmic scales.

conductors,[1,18,22] the p-type semiconductor $MoTe_2$ is essential for several applications, such as p−n junctions and complementary logic circuits. Using the equation for the carrier mobility, $\mu = (dI_{ds}/dV_{bg})(L/W)(1/V_{ds}C_g)$, where L, W, and C_g stand for the channel length and width and the gate capacitance per unit area, respectively, we can estimate the field-effect hole mobility of this $MoTe_2$ FET to be about 1 cm^2 V^{-1} s^{-1}, which is comparable to those of back-gated FETs made from mechanically exfoliated $MoTe_2$ flakes (0.3−10 cm^2 V^{-1} s^{-1}).[12,13] Since these are only two-terminal devices and the effects of Schottky contacts are present, it is anticipated that our few-layer $MoTe_2$ should have better intrinsic transport behavior (e.g., mobility).

The chemical composition of the Mo precursor was found to be crucial for the CVD growth of $MoTe_2$. The resulting $MoTe_2$ phase and the efficiency of the tellurization are both strongly dependent on the oxidation state of the Mo precursor. When Mo (instead of MoO_3) is used as the precursor, a homogeneous 1T′ $MoTe_2$ film (Figure 5a) can also be grown under the same growth conditions as mentioned above. The Raman spectrum of the $MoTe_2$ film shows peaks at 108, 127, 161, 189, and 257 cm^{-1}(Figure 5b). These peak frequencies are consistent with the Raman spectra of bulk 1T′ $MoTe_2$.[17,23] Moreover, the rectangular shape of the SAED pattern (Figure 5c) further verifies that the as-synthesized material is a 1T′ $MoTe_2$ film. The high-resolution XPS spectra for Mo 3d and Te 3d further identify the resulting film after tellurization as being a $MoTe_2$ film. The peaks at 228 and 231.1 eV are assigned to the Mo $3d_{5/2}$ and Mo $3d_{3/2}$ peaks, respectively, of the Mo−Te bonds (Figure 5d). The peaks at 572.6 and 583 eV in Figure 5e correspond to the Te $3d_{5/2}$ and Te $3d_{3/2}$ peaks of $MoTe_2$. Moreover, the Mo:Te atomic ratio is around 1:2, indicating that the 1T′ $MoTe_2$ phase also has good stoichiometry.

We found that MoO_3 reacts more easily with Te and forms 2H $MoTe_2$ under our synthesis conditions. In contrast, Mo and MoO_x ($x < 3$) precursors tend to form 1T′ $MoTe_2$ under the same conditions. Theoretical calculations predict that the energy

DOI: 10.1021/jacs.5b07452
J. Am. Chem. Soc. 2015, 137, 11892−11895

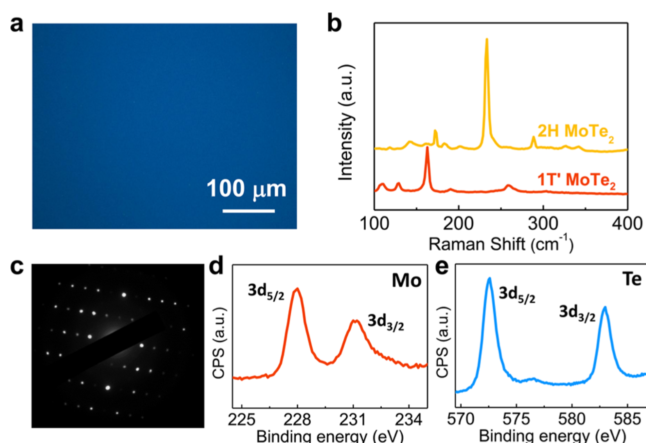

Figure 5. Characterizations of the resulting 1T′ $MoTe_2$ film. (a) Typical optical image of an as-synthesized 1T′ $MoTe_2$ film on 300 nm SiO_2/Si. (b) Raman spectra of 1T′ (red) and 2H (yellow) $MoTe_2$ films. (c) SAED pattern of the 1T′ $MoTe_2$ film. (d, e) High-resolution (d) Mo 3d and (e) Te 3d XPS spectra of a 1T′ $MoTe_2$ film.

difference between the 1T′ and 2H phases of $MoTe_2$ is small and that 1T′ $MoTe_2$ is thermodynamically stable under certain mechanical strain conditions.[16] In view of the drastic change in the volume of each Mo unit in going from Mo (15.6 $Å^3$, 380%) or MoO_2 (32.5 $Å^3$, 130%) to $MoTe_2$ (74.9 $Å^3$), it is likely that a large strain is induced during the transformation from Mo to a $MoTe_2$ film. As a result, the 1T′ phase, which is metastable without strain, becomes the more stable phase for $MoTe_2$ synthesized from a Mo film. In contrast, the change in volume in going from MoO_3 (50.8 $Å^3$) to $MoTe_2$ (74.9 $Å^3$) is about 47%, which is much lower than that for the Mo system. This stress can be relaxed during the high-temperature growth. This might be the reason that 2H $MoTe_2$, which is the more stable phase in the absence of strain, can be obtained by tellurization of MoO_3. Since MoO_3 tends to lose oxygen during evaporation,[24] we first deposited Mo by electron-beam evaporation and then fully oxidized the Mo film in air.

Another key parameter involved in $MoTe_2$ growth is the amount of the Te source. Te vapor should be maintained during the growth of both the 2H and 1T′ phases to avoid Te deficiency in the as-grown film because $MoTe_2$ is unstable and Te is prone to sublime at high temperature.

In summary, we have presented a simple yet very effective technique to produce large-area, atomically thin $MoTe_2$ films. The resulting $MoTe_2$ can be pure 2H phase or pure 1T′ phase with high crystallinity depending on the choice of Mo precursor. The as-grown few-layer $MoTe_2$ films are stoichiometric and have high uniformity. The electrical transport properties of our 2H $MoTe_2$ films are comparable to those of mechanically exfoliated $MoTe_2$ flakes. Since our high-quality, atomically thin $MoTe_2$ films are highly homogeneous and the size of the films is limited only by the size of the substrate, our growth method paves the way for large-scale applications of $MoTe_2$ in the context of high-performance nanoelectronic and optoelectronic devices and circuits.

ASSOCIATED CONTENT

Supporting Information

The Supporting Information is available free of charge on the ACS Publications website at DOI: 10.1021/jacs.5b07452.

Experimental details and supporting figures (PDF)

AUTHOR INFORMATION

Corresponding Authors

*jingkong@mit.edu

*millie@mgm.mit.edu

Notes

The authors declare no competing financial interest.

ACKNOWLEDGMENTS

The authors acknowledge financial support from NSF (Grant DMR-1004147), ONR (Grant N00014-1-1063-09), and the International Postdoctoral Exchange Fellowship Program (Grant 20130002), ARO (Grants W911NF-14-2-0071, 6930265 and 6930861), NSFC (Grant 51272291), MOST (Grant 103-2112-M-007-001-MY3) and MEXT(Grants 25107004 and 25107005).

REFERENCES

(1) Radisavljevic, B.; Radenovic, A.; Brivio, J.; Giacometti, V.; Kis, A. *Nat. Nanotechnol.* **2011**, *6*, 147.

(2) Tan, C.; Zhang, H. *Chem. Soc. Rev.* **2015**, *44*, 2713.

(3) Li, H.; Wu, J.; Yin, Z.; Zhang, H. *Acc. Chem. Res.* **2014**, *47*, 1067.

(4) Wang, Q. H.; Kalantar-Zadeh, K.; Kis, A.; Coleman, J. N.; Strano, M. S. *Nat. Nanotechnol.* **2012**, *7*, 699.

(5) Yin, Z.; Li, H.; Li, H.; Jiang, L.; Shi, Y.; Sun, Y.; Lu, G.; Zhang, Q.; Chen, X.; Zhang, H. *ACS Nano* **2012**, *6*, 74.

(6) Huang, X.; Zeng, Z.; Zhang, H. *Chem. Soc. Rev.* **2013**, *42*, 1934.

(7) Sie, E. J.; McIver, J. W.; Lee, Y.-H.; Fu, L.; Kong, J.; Gedik, N. *Nat. Mater.* **2015**, *14*, 290.

(8) Xu, X.; Yao, W.; Xiao, D.; Heinz, T. F. *Nat. Phys.* **2014**, *10*, 343.

(9) Lukowski, M. A.; Daniel, A. S.; Meng, F.; Forticaux, A.; Li, L.; Jin, S. *J. Am. Chem. Soc.* **2013**, *135*, 10274.

(10) Huang, X.; Zeng, Z.; Bao, S.; Wang, M.; Qi, X.; Fan, Z.; Zhang, H. *Nat. Commun.* **2013**, *4*, 1444.

(11) Ruppert, C.; Aslan, O. B.; Heinz, T. F. *Nano Lett.* **2014**, *14*, 6231.

(12) Lin, Y.-F.; Xu, Y.; Wang, S.-T.; Li, S.-L.; Yamamoto, M.; Aparecido-Ferreira, A.; Li, W.; Sun, H.; Nakaharai, S.; Jian, W.-B.; Ueno, K.; Tsukagoshi, K. *Adv. Mater.* **2014**, *26*, 3263.

(13) Pradhan, N. R.; Rhodes, D.; Feng, S.; Xin, Y.; Memaran, S.; Moon, B.-H.; Terrones, H.; Terrones, M.; Balicas, L. *ACS Nano* **2014**, *8*, 5911.

(14) Abruña, H. D.; Hope, G. A.; Bard, A. J. *J. Electrochem. Soc.* **1982**, *129*, 2224.

(15) Nicolosi, V.; Chhowalla, M.; Kanatzidis, M. G.; Strano, M. S.; Coleman, J. N. *Science* **2013**, *340*, 1226419.

(16) Duerloo, K.-A. N.; Li, Y.; Reed, E. J. *Nat. Commun.* **2014**, *5*, 4214.

(17) Park, J. C.; Yun, S. J.; Kim, H.; Park, J.-H.; Chae, S. H.; An, S.-J.; Kim, J.-G.; Kim, S. M.; Kim, K. K.; Lee, Y. H. *ACS Nano* **2015**, *9*, 6548.

(18) Wang, X.; Gong, Y.; Shi, G.; Chow, W. L.; Keyshar, K.; Ye, G.; Vajtai, R.; Lou, J.; Liu, Z.; Ringe, E.; Tay, B. K.; Ajayan, P. M. *ACS Nano* **2014**, *8*, 5125.

(19) Yamamoto, M.; Wang, S. T.; Ni, M.; Lin, Y.-F.; Li, S.-L.; Aikawa, S.; Jian, W.-B.; Ueno, K.; Wakabayashi, K.; Tsukagoshi, K. *ACS Nano* **2014**, *8*, 3895.

(20) Guo, H.; Yang, T.; Yamamoto, M.; Zhou, L.; Ishikawa, R.; Ueno, K.; Tsukagoshi, K.; Zhang, Z.; Dresselhaus, M. S.; Saito, R. *Phys. Rev. B: Condens. Matter Mater. Phys.* **2015**, *91*, 205415.

(21) Bernède, J. C.; Amory, C.; Assmann, L.; Spiesser, M. *Appl. Surf. Sci.* **2003**, *219*, 238.

(22) Liu, W.; Kang, J.; Sarkar, D.; Khatami, Y.; Jena, D.; Banerjee, K. *Nano Lett.* **2013**, *13*, 1983.

(23) Keum, D. H.; Cho, S.; Kim, J. H.; Choe, D.-H.; Sung, H.-J.; Kan, M.; Kang, H.; Hwang, J.-Y.; Kim, S. W.; Yang, H.; Chang, K. J.; Lee, Y. H. *Nat. Phys.* **2015**, *11*, 482.

(24) Chuang, S.; Battaglia, C.; Azcatl, A.; McDonnell, S.; Kang, J. S.; Yin, X.; Tosun, M.; Kapadia, R.; Fang, H.; Wallace, R. M.; Javey, A. *Nano Lett.* **2014**, *14*, 1337.

DOI: 10.1021/jacs.5b07452
J. Am. Chem. Soc. 2015, 137, 11892−11895